Inorganic Chemistry
Article
Cite This: Inorg. Chem. 2019, 58, 7069−7077
pubs.acs.org/IC

Mössbauer Spectroscopy and Theoretical Studies of Iron Bimetallic Complexes Showing Electrocatalytic Hydrogen Evolution

Codrina V. Popescu,*[,†] Shengda Ding,[‡] Pokhraj Ghosh,[‡] Michael B. Hall,*[,‡] and Morgan Cohara[§]

[†]Department of Chemistry, University of St. Thomas, St. Paul, Minnesota 55105, United States
[‡]Department of Chemistry, Texas A&M University, College Station, Texas 77843, United States
[§]Department of Chemistry, Colgate University, Hamilton, New York 13346, United States

Supporting Information

ABSTRACT: Mössbauer spectroscopy and density functional theory (DFT) calculations are reported for the mononuclear Fe−nitrosyl complex [Fe(*N*,*N*′-bis(2-mercaptoethyl)-1,4-diazacycloheptane)NO] {[Fe(bme-dach)(NO)] (**1**)} and the series of dithiolate-bridged dinuclear complexes M-Fe(CO)Cp [M = Fe(bme-dach)(NO) (**1-A**), Ni(bme-dach) (**2-A**), and Co(bme-dach)(NO) (**3-A**)], in which M is a metallo-ligand to Fe(CO)Cp$^+$ (Fe′$_{Cp}$). The latter is an organometallic fragment in which Fe is coordinated by one CO and one cyclopentadienyl ligand. Complexes **1-A** and **2-A** were previously shown to have electrocatalytic hydrogen evolution activity. Mononuclear {Fe-NO}^{7} complex **1**, with overall spin of $^1/_2$, has an isomer shift of 0.23(2) mm/s [ΔE_Q = 1.37(2) mm/s] and magnetic hyperfine couplings of {−38 T, −26.8 T, 8.6 T}. In complexes **2-A** and **3-A**, Fe′(CO)Cp$^+$ has a diamagnetic ground state and δ = 0.33(2) mm/s ($\Delta E_Q \approx$ 1.78 mm/s), consistent with a low-spin Fe^{II} site. In contrast, in complex **1-A**, M = Fe(bme-dach)(NO) (i.e., complex **1**) the magnetic hyperfine interactions of both metallo-ligand, M, and low-spin Fe′$_{Cp}$ are perturbed and Fe′$_{Cp}$ exhibits small magnetic hyperfine interactions, although its isomer shift and quadrupole splittings are largely unaltered. The DFT calculations for **1-A** are in agreement with the paramagnetism observed for the Fe′(CO)Cp$^+$ iron site.

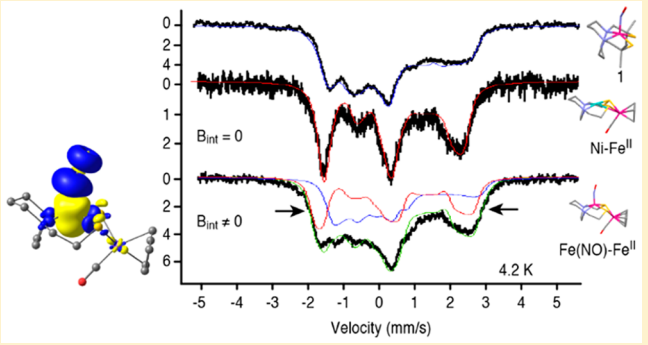

INTRODUCTION

As a radical molecule with unique structure, reactivity, and biological function identified since the 19th century,[1] nitric oxide has been a subject of intense investigation related to all life sciences. Endogenous nitric oxide is involved in numerous cellular processes, such as cell signaling, vasodilation, and inflammation, while at high concentrations, it is a cytotoxic agent against cancer cells.[2−5] NO has also been employed as an exogenous ligand to probe the structure and spectroscopy of non-heme iron-NO complexes. Stable non-heme iron-NO complexes have been examined with spectroscopy as analogues of dioxygen intermediates in mechanisms of O_2 activation and because they are directly relevant to enzymes such as the nitric oxide reductases.[6,7]

Due to the ability of the NO radical molecule to participate in spin coupling and electron transfer when bound to iron, Fe-NO complexes have complicated electronic structures worthy of spectroscopic exploration.[8] Fe-nitrosyl complexes are designated using the Enemark−Feltham notation {Fe-NO}^{n}, which indicates the total number of valence electrons in the Fe (d) and NO (π^*) orbitals.[9] {Fe-NO}^{7} complexes resulting from binding NO to high-spin non-heme Fe(II) complexes have typically an $S = {}^3/_2$ ground state in which the spin state of the iron is $S_{Fe} = {}^5/_2$, which is coupled antiferromagnetically to S = 1 from NO.[10] Five- and six-coordinated {Fe-NO}^{7} complexes with $S = {}^1/_2$ ground states have also been reported, but the electronic configuration of the iron depends on the local ligand environment of the iron that can determine the unpaired electron to be on the NO or on the Fe, leading to different spin states for the Fe ion and to oxidation levels, including Fe(I)-NO$^+$, Fe(II, S = 0)NO, Fe(III, $S = {}^1/_2$)NO$^-$, and Fe(III, $S = {}^3/_2$)NO$^-$.[10−12]

The ability of {Fe-NO}^{7} and DNIC complexes to serve as building blocks in larger structures with interesting properties has been explored in previous papers from the Darensbourg group.[13] For instance, it was demonstrated that some binuclear complexes containing metal-nitrosyl fragments are electrocatalysts for proton reduction.[14−16] In two separate instances, the metallodithiolate species MN_2S_2 [here N_2S_2 is bme-dach (Figures 1 and 2)] serves as a redox active metallo-ligand to an iron-containing electron-accepting unit.

The family of complexes studied here was obtained by coupling the MN_2S_2 complex [M = Fe(NO), Ni, or Co(NO)] through the two thiolate ligands to the low-spin iron(II) organometallic unit FeCp(CO)$^+$, yielding the set of bimetallic

Received: March 14, 2019
Published: May 6, 2019

Downloaded via TEXAS A&M UNIV COLG STATION on June 23, 2021 at 21:23:10 (UTC).
See https://pubs.acs.org/sharingguidelines for options on how to legitimately share published articles.

© 2019 American Chemical Society

DOI: 10.1021/acs.inorgchem.9b00746
Inorg. Chem. 2019, 58, 7069−7077

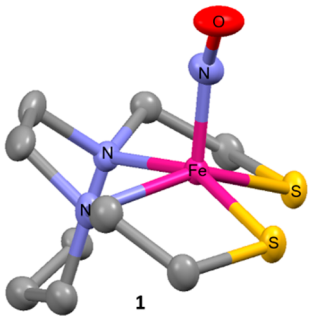

Figure 1. Structure of complex **1**, Fe(bme-dach)NO.[14]

complexes of **1-A**, **2-A**, and **3-A**, shown in Figure 2.[17] In previous studies, a different set of compounds was obtained by coupling the metallo-ligand (bme-dach)Fe(NO) complex to an $Fe(NO)_2$ unit generating the dinuclear complex **1**-$Fe(NO)^{2+}$ (not shown[16]).

In this paper, Mössbauer spectroscopic studies are presented for the mononuclear metallo-ligand (bme-dach)Fe(NO) (Figure 1) and the series of bimetallics **1-A**, **2-A**, and **3-A**. In **1-A**, the iron of metallo-ligand **1** is termed FeNO, while the $Fe(CO)Cp^+$ is called Fe'_{Cp} for the sake of brevity. In the published electrocatalysis experiments, di-iron complex **1-A** showed hydrogen generating capacity, which prompted the study of the mechanism enabling H^+ reduction, drawing parallels with the native enzymes and with other catalysts published recently.[16,18] In short, electrochemical and computational studies showed that **1-A** maintains the hemilability of the thiolate-metal dative bond, which opens when necessary to accommodate proton(s), electron(s), and hydride(s). The parent {Fe-NO}^{7} complex **1** has an $S = {}^1/_2$ ground state, presenting an EPR spectrum with g values 2.088, 2.083, and 2.031. Several bonding schemes could be proposed, including antiferromagnetically coupled $\{Fe^{3+}(d^5, S = {}^1/_2)NO^- (S = 1)\}$, $\{Fe^{3+}(d^5, S = {}^3/_2)NO^\bullet (S = 1)\}$. A complex related to **1**, namely (bme-daco)FeNO, was previously characterized with crystallography and other methods, except Mössbauer spectroscopy.[19] Sun et al.[7] analyzed its sulfur K-edge X-ray absorption spectra (XAS) and conducted density functional theory (DFT) calculations, which led them to conclude that the intermediate-spin Fe^{III} (d^5, $S = {}^3/_2$) would be the best electronic structural description for this complex. This study provides the Mössbauer spectroscopic analysis, yielding fundamental electronic parameters, such as oxidation states, spin states, and hyperfine interactions in bimetallics **1-A**–**3-A** and the parent compound **1**. One of the findings in this paper is the presence of hyperfine interactions on the low-spin Fe^{II} ($S = 0$) site Fe'_{Cp} in **1-A**, which are not present in the other two bimetallic complexes

MATERIALS AND METHODS

Mössbauer Measurements. Low-field (0.07 T), variable-temperature (5–200 K) Mössbauer spectra were recorded on a closed-cycle refrigerator spectrometer (model CCR4K) equipped with a 0.07 T permanent magnet, maintaining temperatures between 5 and 300 K (SeeCo, Edina, MN, seeco.net). MB spectra in strong applied magnetic fields (1.0–8.0 T) were recorded on liquid helium-cooled superconducting magnet instruments at the National Magnet Lab (University of Florida, S. Stoian) and at Carnegie Mellon University (A. Guo). Mössbauer spectra were analyzed using the software WMOSS (Ion Prisecaru, wmoss.org) and Spin Count (M. Hendrich, Carnegie Mellon University). The samples were polycrystalline powders, suspended in nujol, placed in Delrin 1.00 mL cups, and frozen in liquid nitrogen. The isomer shifts are quoted at 6 K, with respect to iron metal standard spectra recorded at 298 K. Spectral simulation and least-squares fits were produced using the quadrupole interaction Hamiltonian in eq 1 appended with the spin Hamiltonian for electronic spins $S = {}^3/_2$ (eq 2a, for the intermediate-spin ferric ion) and $S = {}^1/_2$ (eq 2b, for the low-spin simulations).

$$\hat{H}_Q = \frac{eQV_{zz,i}}{12}\left[\hat{I}_{z,i}^{\,2} - \frac{15}{4} + \eta(\hat{I}_{x,i}^{\,2} - \hat{I}_{y,i}^{\,2})\right] \tag{1}$$

$$\widehat{H_{IS}} = D\left[S_z^{\,2} - \frac{1}{3}S(S+1) + \frac{E}{D}(S_x^{\,2} - S_y^{\,2})\right] + \beta\hat{\mathbf{S}}\cdot\tilde{\mathbf{g}}\cdot\vec{\mathbf{B}} + \hat{\mathbf{S}}\cdot\tilde{\mathbf{A}}_i\cdot\hat{\mathbf{I}} + \hat{H}_Q(i) - g_n\beta_n\vec{\mathbf{B}}\cdot\hat{\mathbf{I}} \tag{2a}$$

$$\widehat{H_{LS}} = \beta\hat{\mathbf{S}}\cdot\tilde{\mathbf{g}}\cdot\vec{\mathbf{B}} + \hat{\mathbf{S}}\cdot\tilde{\mathbf{A}}_i\cdot\hat{\mathbf{I}} + \hat{H}_Q(i) - g_n\beta_n\vec{\mathbf{B}}\cdot\hat{\mathbf{I}} \tag{2b}$$

Simulations of high-field Mössbauer spectra in which exchange coupling was considered used the $H_{ex} = \mathbf{J}\cdot S_1 S_2$ Hamiltonian where $J > 0$, which indicates the $m_S = 0$ doublet is the ground state (antiferromagnetic).

Computational Methodology. The functional B3LYP[20] was used in ORCA 3.0.2[21] to compute all of the calculations. The triple-ζ 6-311++G(d,p) basis set was used for all non-metal atoms,[22−24] and a Wachters-Hay basis set with diffuse functions and polarization functions, under the designation 6-311++G(d,p), was used for transition metals.[3,25−28] The crystal structures of **1-A**$^+$, **1-B**$^+$, and **1-C**$^+$ were imported as references. The crystal structure of the free metallo-ligand **1** was also imported but symmetrized to C_s symmetry before further processes. All of the stationary points are optimized in the gas phase and verified by frequency calculations with appropriate numbers of imaginary vibrations. The orbitals are localized by the Foster–Boys method if necessary.[25]

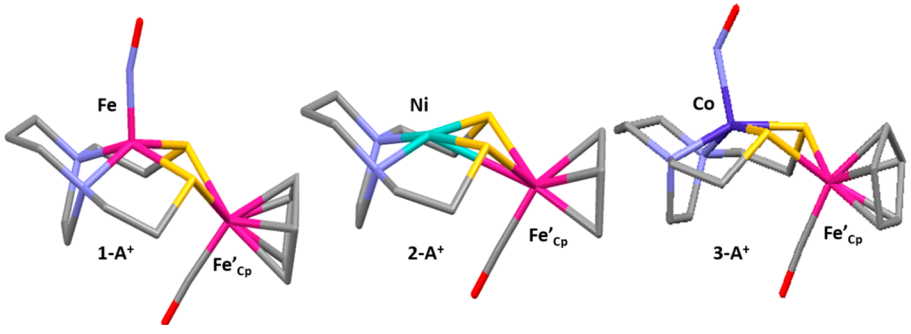

Figure 2. Structures of the cations of dinuclear complexes **1-A**, **2-A**, and **3-A**, in which complex **1** is a metallo-ligand. The BF_4^- counterion has been omitted for the sake of clarity; Fe is colored magenta, Ni cyan, and Co purple.

DOI: 10.1021/acs.inorgchem.9b00746
Inorg. Chem. 2019, 58, 7069−7077

RESULTS

Mössbauer Spectra of Compound 1. The low-field variable-temperature spectra of compound **1** (Figure 3 and Table 1) were fitted with a single sharp quadrupole doublet, with δ = 0.23 ± 0.02 mm/s and ΔE_Q = 1.35 ± 0.02 mm/s. While compatible with either low- or intermediate-spin Fe(III) or Fe(II), these parameters cannot unambiguously determine the oxidation state without a discussion of the high-field Mössbauer data (see below).

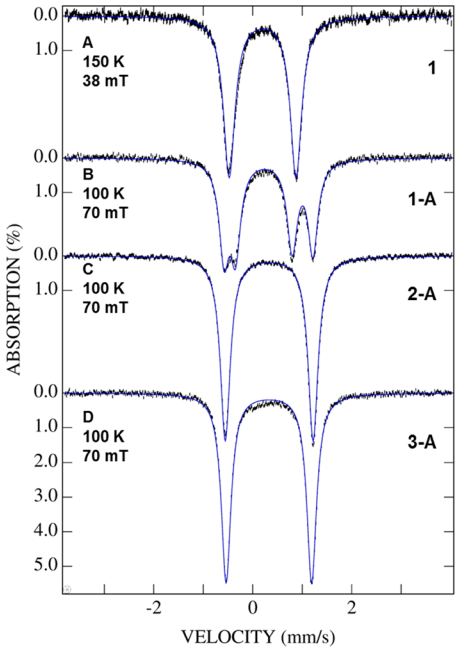

Figure 3. Mössbauer spectra (hash marks) and spectral simulations (blue line) in low applied magnetic fields at temperatures of 150 K (A, complex 1) and 100 K (B–D, complexes **1-A**, **2**-A, and **3-A**, respectively).

The spectra of **1** in large applied magnetic fields of strengths between 100 mT and 8 T are shown in Figure 4. These spectra present distinct patterns of splittings that are due to interaction of the nuclear spin with the electronic spin, consistent with a paramagnetic electronic ground state. Thus, the Mössbauer data exclude a low-spin ferrous ion with an S = 0 ground state. The variable-field Mössbauer spectra in Figure 4 were analyzed

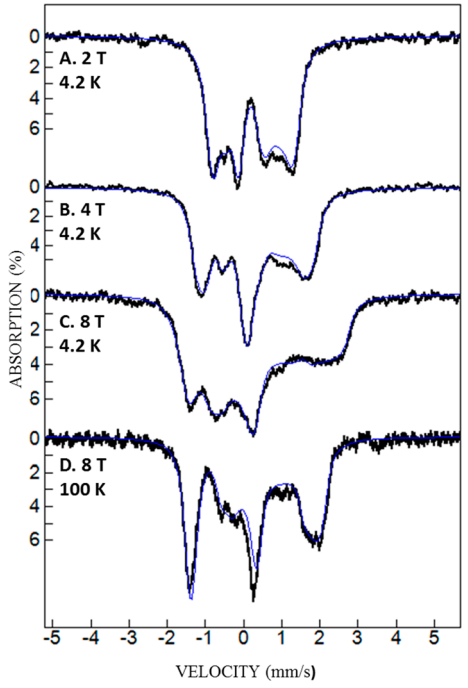

Figure 4. Variable-field, variable-temperature Mössbauer spectra (hash marks) of complex **1**, in polycrystalline powder suspended in mineral oil. The solid lines are spectral simulations with an $S = {}^1/_2$ electronic spin, with the parameters listed in Table 1. The intrinsic line widths are 0.30 mm/s.

with the assumption of an $S = {}^1/_2$ ground state for the {Fe-NO}^{7} system, consistent with the low-temperature EPR spectra published in previous reports showing an isotropic signal (see Table 2) with strong ^{14}N hyperfine interactions at the NO. Figure 4 shows the fits assuming fast relaxation of the electronic spin on the Mössbauer time scale (appropriate for powders and concentrated solutions) obtained by simultaneous fitting of the spectra in applied fields varying between 1.0 and 8.0 T. While the low-field data do not indicate impurities, the high-field spectra present broad paramagnetic features, which can be fit roughly but not perfectly with a single species suggesting some heterogeneity in the sample in terms of the magnetic hyperfine interactions. Keeping all parameters constant but allowing two species with different Euler angles, we obtained the best fits in Figure 4 with the major species

Table 1. ^{57}Fe Mössbauer Parameters for Complexes 1, 1-A, 2-A, and 3-A

	1	1-A		2-A	3-A
	N_2S_2FeNO	$N_2S_2Fe(NO)$	$Fe'Cp(CO)^+$	$Fe'Cp(CO)^+$	$Fe'Cp(CO)^+$
S	${}^1/_2$	${}^1/_2$	0	0	0
δ (mm/s) (4.2 K)	0.23(2)	0.23(2)	0.34(2)	0.33(2)	0.33(2)
ΔE_Q (mm/s)					
4.2 K	1.37(2)	1.15	1.79	1.78(2)	1.75(2)
100 K	1.25(5)	1.0	1.50		
α, β, γ	Sp.1 (90%) (0, 17, 0)				
	Sp.2 (10%) (65, 0, 0)				
η	0	0	0.7	0.3	0
$A_{x,y,z}/g_n\beta_n$ (T)	−38, −23.8, 8.6	−35(1), −20(1), 1.3(1)	0, 2, 4		
α', β', γ'	Sp.1 (90%) (0, 0, 0)				
	Sp.2 (10%) (90, 0, 0)				
Γ (mm/s)	0.30	0.30	0.30	0.30	0.30

DOI: 10.1021/acs.inorgchem.9b00746
Inorg. Chem. 2019, 58, 7069–7077

Table 2. Mössbauer and EPR Parameters of 1, 1-A, and Relevant Literature NO Complexes

	S_{tot}	S_{Fe}	δ (mm/s)	ΔE_Q (mm/s)	g values ^{14}N, A (G)	$A_{x,y,z}/g_N\beta_N$ (T)	ref
1	$^1/_2$	$^3/_2$	0.23	1.37	2.074, 2.042, 2.0038[c]	−38	this work
Fe(bme-dach)NO					24.7, 9.4, 21.3 (90%)[c]	−23.8	16
					44.9, 16.4, 41.8 (10%)[c]	8.6	
1-A	$^1/_2$	$^3/_2$	0.23	1.15	2.04 (15.3 G)	−35	this work
Fe(bme-dach)NO						−20	
						1.3	
trans-cyclamFe(NO)Cl]$^+$	$^1/_2$	$^3/_2$	0.27	1.26	2.052, 2.0145, 1.9698 (117, 53, 64 G)	−23[a]	11
O_h (6)						−13.7	
						11.9	
Fe(TPP)(NO)	$^1/_2$	–	0.35	1.24	2.085, 2.032, 2.01 (24, 16.5, 16 G)	−25	29
square pyramid (5)						−10	
						13.2	
Fe(NO)(TC-5,5)	$^1/_2$	$^1/_2$	0.06[b]	1.39	2.11, 2.03, 2.01	not applicable	30
square pyramid (5)							
[Fe1^R(NO)]-Trig Bipy (5)	$^3/_2$	$^5/_2$	0.412	1.336	4.41, 3.57, 2.00	not applicable	31
[Fe(TMG$_3$tren)(NO)](OTf)$_2$ (5)	$^3/_2$	$^5/_2$	0.48	1.42	4.41, 3.59, 1.97	not applicable	13, 32, 33

[a] $A^{eff}/g_n\beta_n$ = −23.4, −13.7, 11.9 T. [b] This value was determined at 77 K. All other isomer shifts are at 4.2 K. [c] EPR spectra at 10 K (Hauser et al.[11]); EPR spectra at 298 K (Hsieh et al.[16]).

contributing 90% of the spectrum. For this major species, all of the tensors are collinear, which is the premise we used further in analyzing the complex. The essential features of the spectra (Figure 4) are decided by two parameters, the positive electric-field gradient and the magnetic hyperfine tensor components, $A_{x,y,z}$. The 2.0 − T spectrum (Figure 4A) shows incipient magnetic splittings, having two distinct groups of lines of almost equal intensity. The high-energy side of this spectrum is a broadened feature originating from the Mössbauer transitions to the $m_I = \pm^3/_2$ doublet of the $I = {}^3/_2$ excited state. The relatively small broadening seen in this feature shows that at this applied magnetic field the nuclear Zeeman interaction given by $g_n\beta_n(\mathbf{B_{app}} + \mathbf{B_{int}})$ is small compared to the quadrupole splitting, because the V_{zz} axis is roughly aligned with a small $\mathbf{B_{int}}$ component. As the applied magnetic field increases (Figure 4B,C), the high-energy lines develop in the broad feature between 0.5 and 2 mm/s at 8.0 T. The shape of the 100 K spectrum indicates a positive sign for V_{zz}, which is confirmed by the simultaneous fitting with a spin Hamiltonian of the whole data set.

Mössbauer Spectra of Dinuclear Complex 1-A. Complex **1-A** exhibits two quadrupole doublets at all temperatures studied between 4.2 and 200 K. The two spectral components of **1-A** remain distinct up to 200 K, showing valence-localized ions. As shown by the structures in Figures 1 and 2, the N_2S_2 (bme-dach) ligand in complex **1** was used as a carrier of different metal ions to construct complexes **1-A**, **2-A**, and **3-A**, which have the Fe′$_{Cp}$ site in common. By examination of the quadrupole doublets in panels A and B of Figure 3, it is observable that under low applied magnetic fields the spectrum of **1-A** is almost a superposition of the spectra of the mononuclear **1** and the low-spin ferrous Fe′$_{Cp}$ center from **2-A**. As complexes **2-A** and **3-A** contain non-iron metallo-ligands in the N_2S_2 moiety, their Mössbauer spectra consist of the isolated contribution of the Fe′$_{Cp}$ center. The isomer shifts of the Fe′(CO)Cp$^+$ center in dinuclear complexes **1-A**, **2-A**, and **3-A** are identical within 0.01 mm/s at $\delta_{\mathbf{1\text{-}A+}}$ = 0.34 and $\delta_{\mathbf{2\text{-}A+}} = \delta_{\mathbf{3\text{-}A+}}$ = 0.33 mm/s (Table 1), implying that this ion is largely electronically isolated from the metallo-ligand. The isomer shifts of **2-A** and **3-A** are in the range of low-spin ferrous complexes with cyclopentadienyl ligands and consistent with the presence of the thiolate donors.[34]

The Mössbauer spectra in high applied magnetic fields of complex **1-A** are shown in Figure 5. According to the structure, complex **1-A** consists of complex **1** and the organometallic complex Fe′(CO)(cyclopentadienyl), which in complexes **2-A** and **3-A** presents a diamagnetic high-field Mössbauer spectrum (Figure 6). The isomer shifts and quadrupole splittings of complexes **1** and **1-A** are practically identical; thus, we have

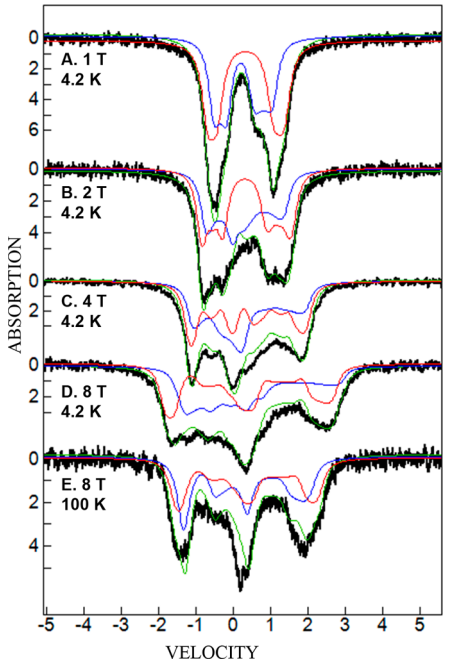

Figure 5. Variable-field, variable-temperature Mössbauer spectra of complex **1-A**. The hash marks are experimental data; solid lines are simultaneous spectral fits with one electronic spin $S = {}^1/_2$ interacting with both Fe nuclei. The subspectrum of the [FeNO] ($S = {}^1/_2$) is colored blue, and that of Fe′$_{Cp}$ ($S = 0$) red. The green line is the sum of the two subspectra with equal contributions with the parameters listed in Table 1.

DOI: 10.1021/acs.inorgchem.9b00746
Inorg. Chem. 2019, 58, 7069−7077

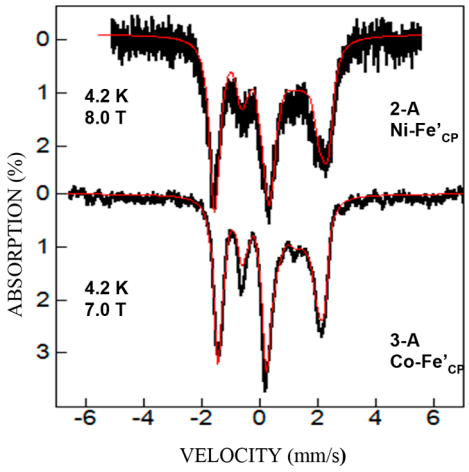

Figure 6. 4.2 K Mössbauer spectra of the Fe'_{Cp} site in complexes (A) **2-A** and (B) **3-A**. The hash marks are experimental data, and solid lines are spectral fits with $S = 0$ ground states and parameters listed in Table 1.

used the description of complexes **1** and of that of the Fe′(CO)(cyclopentadienyl) from complex **2-A** for an initial analysis of complex **1-A** (Figure SI-3) which fitted the data poorly. Closer analysis of the high-field spectra revealed that they could not be satisfactorily simulated with a simple superposition of the two isolated components, one for compound **1** (metallo-ligand) and the other for a low-spin Fe^{II} compound, Fe'_{Cp}. Namely, the assumption that one can add the spectrum of complex **1** to a spectral component representing Fe'_{Cp} with a diamagnetic ground state (each with equal contribution) does not produce acceptable simulations for the series of spectra in large applied magnetic fields for **1-A**. Therefore, we have considered the possibility of weak magnetic hyperfine interactions observed at the low-spin ferrous center, by assuming an effective $S = {}^1/_2$ system, with magnetic hyperfine interactions on both irons. Simultaneous fits of the spectra in strong applied magnetic fields between 1 and 8 T were obtained by adding two subspectra: one contributed by the [FeNO] moiety and a second contributed by the Fe'_{Cp} site, which was allowed to have small internal fields from coupling with the electronic spin on the [FeNO]. This model (Figure 5) yielded the parameter set in Table 1. Inspection of Figure 5 allows observation of the subspectrum of [FeNO] (blue), which contributes the inner features of the dimer's experimental spectrum, while the subspectrum of Fe'_{Cp} (red) contributes the outer features of the spectrum, due to its larger electric field gradient.

The outer splitting of the experimental spectrum was matched, introducing internal fields at the Fe'_{Cp} nucleus corresponding to $A_y = 2$ T and $A_z = 4$ T. The **A** tensor of the $[Fe^{III}NO]$ moiety for the dimer obtained in this procedure has an isotropic part at approximately −15 T, which is reduced by approximately 17% in comparison with that of the Fe^{III} center in complex **1**.[11]

Mössbauer Spectra in High Applied Magnetic Fields of Complexes 2-A and 3-A. For low-spin sites, isomer shifts alone are not definitive indicators of oxidation state; thus, to distinguish between low-spin Fe^{II} and Fe^{III}, it is necessary to establish the ground spin state. This was accomplished by examining 4 K spectra in strong applied fields. Simulations of the high-field spectra of both **2-A** and **3-A** (Figure 6) show that the only splittings present can be attributed to the nuclear Zeeman interaction; that is, the iron nucleus does not experience internal fields, consistent with diamagnetic ($S = 0$) electronic ground states. On the basis of the isomer shift and diamagnetism, the Fe'_{Cp} half of these complexes was identified as a low-spin Fe^{II} ion.

COMPUTATIONAL STUDY

Computational protocols were applied to analyze the electronic structures and predict spectral properties. The crystal structures of the metallo-ligand **1** and bimetallic compounds **1-A**, **2-A**, and **3-A** were imported as the geometric references. Group symmetry C_s was adopted to simplify the calculations. The calculated metric parameters of three bimetallics are provided in Table SI-1 as a validity check; further details of the computational methodology can be found in the Supporting Information.

The metallo-ligand **1** has seven shared electrons between the iron and the nitrosyl, as represented by the Enemark−Feltham notation $\{Fe\text{-}NO\}^7$,[9] and was determined to have a doublet ground state by previous experimental[14,19,35] and theoretical work.[7] One unpaired electron may satisfy the multiplicity requirement, but significant spin polarization (Figure 7), i.e.,

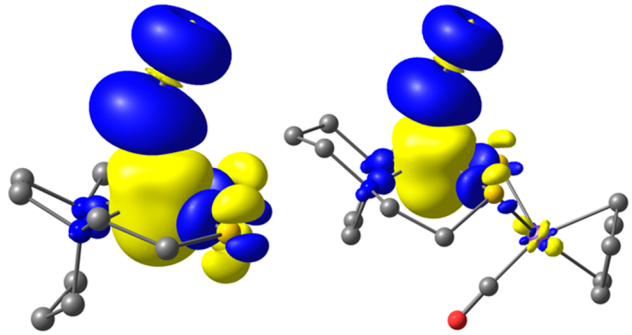

Figure 7. Spin density plots of **1** (left) and **1-A** (right).

spin densities of 2.044 on Fe and −1.100 on NO, was predicted by the functional B3LYP,[36] consistent with previous results by Sun et al.[7] and our own studies,[16] indicating the presence of more than one unpaired electron. The localized Fe-NO back-bonding orbitals, by the Foster−Boys method[25] to exclude the S π-donation mixing, are presented in Figure 8. The relevant α and β electrons are accommodated in orbitals with significant different contributions from Fe and NO such that the α electrons can be qualitatively assigned to the iron and the β electrons can be qualitatively assigned to the nitrosyl. Therefore, the configuration is best represented as $(\text{Fe-d}_{xy})^2(\text{Fe-d}_{xz})^\alpha(\text{NO-}\pi^*_x)^\beta(\text{Fe-d}_{yz})^\alpha(\text{NO-}\pi^*_y)^\beta(\text{Fe-d}_{z^2})^\alpha$ rather than $(\text{Fe-d}_{xy})^2(\text{Fe-d}_{xz})^2(\text{Fe-d}_{yz})^2(\text{Fe-d}_{z^2})^\alpha$ to match the overwhelming NO contributions in the β-back-bonding orbitals. The overall doublet $\{Fe\text{-}NO\}^7$ is achieved by the antiferromagnetic coupling of an intermediate-spin ($S = {}^3/_2$) Fe^{III} and a high-spin ($S = -1.0$) NO^-, consistent with the interpretation of the Mössbauer spectroscopic results (see Discussion). This electron configuration can be compared with that of another five-coordinated $\{Fe\text{-}NO\}^7$ complex $Fe(TMG_3tren)(NO)](OTf)_2$, where the Fe-NO bond was similarly covalent and dominated by the π-donating character of the NO^-.[33] However, in the trigonal bipyramidal geometry of the cited complex, the $d_{x^2-y^2}$ orbital would be more accessible than in the square-planar case of complex **1**.

DOI: 10.1021/acs.inorgchem.9b00746
Inorg. Chem. 2019, 58, 7069−7077

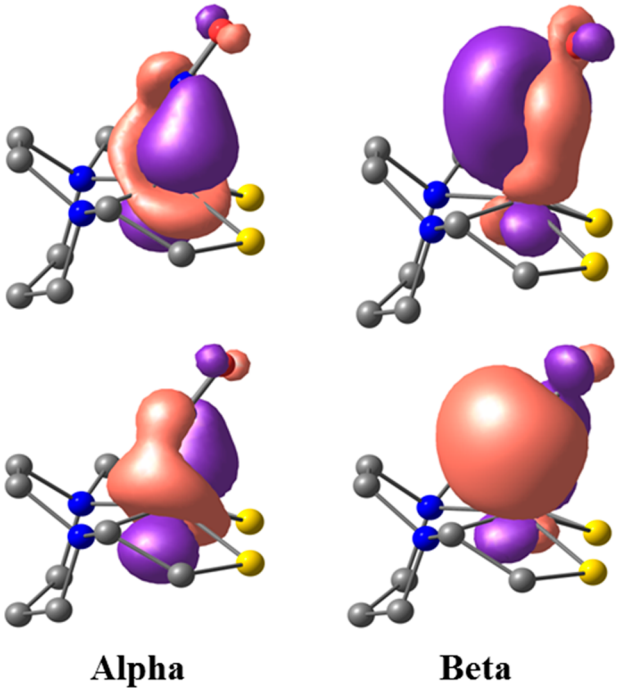

Figure 8. Spin-polarized Fe-NO back-bonding of **1** as presented by Foster−Boys localized orbitals. The α spin orbitals are recognized as Fe lone pairs, while the β spin orbitals as Fe−N bonds with significantly more contributions from NO, as indicated by the localization analysis.

It should be noted that the extent of predicted spin polarization is functionally dependent and is more significant for the high-spin favoring hybrid functional B3LYP than the low-spin favoring pure functional TPSS.[37] A full CASSCF calculation assessing the multireference property of the $\{Fe\text{-}NO\}^{7/8}$ moiety in the N_2S_2 coordination environment is currently underway. The attachment of the closed-shell fragment $Fe'(CO)Cp^+$ to the metallo-ligand **1** to form **1-A** does not cause *de facto* alterations to the antiferromagnetic coupling scheme of the $\{Fe(NO)\}^7$ fragment (Figure 7). It even simplifies orbital analysis because two thiolate S lone pairs are utilized to chelate Fe'_{Cp} and the unfavorable orbital mixture in the canonical orbitals (not presented) is eliminated. In spite of the low-spin nature of Fe'_{Cp}, which would prescribe a ground spin state of zero, a small residue spin density of 0.020 was found (Figure 7) The calculated hyperfine coupling constants are listed in Table SI-2. This theoretical prediction is in agreement with the experimental finding presented in the previous section.

DISCUSSION

This Mössbauer study aims to provide an understanding of the fundamental electronic properties of sulfur-bridged bimetallic $N_2S_2M\text{-}Fe'(CO)Cp$ complexes [M = FeNO (**1-A**), Ni^{II} (**2-A**), or CoNO (**2-A**)]. The dinuclear complexes feature a constant organometallic building block, containing a low-spin center and the metallo-ligand N_2S_2 featuring Fe-NO, Ni, and Co-NO. Complex **1** was studied to ascertain the Mössbauer spectral behavior of complex **1-A**, which presented hyperfine interactions on both iron centers. The DFT calculations predicted correctly the experimental signs and relative magnitudes of the **A** tensor components for [Fe-NO] in both **1** and **1-A**, although the magnitudes are slightly overestimated (Table SI-3).

A complex almost identical to **1** was studied by Sun et al.,[7] who concluded that its $S = {}^1/_2$ ground state results from the spin coupling of an intermediate-spin Fe^{III} ($S_{Fe} = {}^3/_2$) with a nitroxide ion (NO^- with $S_{NO} = 1$). From the study presented here, the isomer shift of 0.23 mm/s of **1** and the $S = {}^1/_2$ electronic ground state indicated by EPR are inconsistent with high-spin configurations (examples are listed in Table 2); thus, the principal candidates for oxidation states are low-spin and intermediate-spin Fe^{III}. The Mössbauer data of both complexes **1** and **1-A** are fitted with the overall $S = {}^1/_2$ spin system, but some of the features of the paramagnetic spectra of **1** are not entirely consistent with the assignment of a low-spin configuration for these Fe^{3+} sites. Furthermore, the DFT calculations above reproduce well the experimental g values [2.088, 2.067, 2.03 (Table SI-3)] with a model in which the iron has $S_{Fe} = {}^3/_2$ and it is coupled to NO^- ($S_{NO} = 1$). The spectral features and parameters of **1** are similar to those of mononuclear complexes *trans*-$[cyclamFe^{III}(NO)Cl]^+$ and $[Fe^{III}Cl(cyclam\ ac)]^+$ for which $S = {}^3/_2$ ground states (Table 2) were assigned on the basis of variable-field Mössbauer and DFT calculations.[11,38] From the Mössbauer data in this study, two arguments can be brought against the presence of a low-spin ferric ion in **1**. First, the EFG for a low-spin Fe^{III} ion exhibiting the g values of this complex (Table 1) would have the unpaired electron in a t_{2g}-type Fe^{3+} orbital that is well above the other orbitals in the t_{2g} set. This is well-known to produce negative V_{zz} values and therefore negative quadrupole splittings, unlike the quadrupole splitting seen for complexes **1** and **1-A**.[11,38−41] Second, if this were a low-spin Fe^{III} bound to an NO radical species, to obtain a total spin of ${}^1/_2$, one would assume an antiferromagnetic coupling between $S_{Fe} = {}^1/_2$ and $S_{NO} = 1$. This would be a plausible scenario, provided that the sign of the magnetic hyperfine components predicted by this coupling scheme would agree with the signs observed in the Mössbauer spectral fits. Thus, we must consider the two spin coupling cases, and for each of them, we will discuss the sign and relative magnitude of the average magnetic hyperfine couplings (A-values). The isotropic component of the hyperfine tensor of **1** can be estimated from the trace of the experimentally obtained **A** tensor, and it is $A_{iso} \approx -17$ T. We note that this value is lower than the isotropic part of the typical octahedral "ionic" Fe^{III} (−22 to −20 T),[42] but consistent with the smaller coordination number and the presence of sulfur donors for which a higher degree of bond covalency is expected. The A_{iso} value for **1** is comparable to that of Fe−S clusters, approximately −16.5 T,[43] and also similar to the A_{iso} reported for non-heme complexes with similar coordination (−16 T).[11,38,44]

In coupling $S_{Fe} = {}^1/_2$ with $S_{NO} = 1$, the nitroxide spin is the larger spin; therefore, the resultant spin will have the sign and vector direction of S_{NO}. Thus, the effective A values of the coupled system are given by the formula

$$A_{i\text{eff}}(\text{Fe}-\text{NO}) = A_{\text{eff}}(\text{Fe}) + A_{\text{eff}}(\text{NO}) = (-1/3)A_{\text{Fe},i} + (4/3)A_{(\text{NO}),i}$$

in which the effective value of A_{NO} has a positive larger projection coefficient and the A values of the Fe(III) have a negative and smaller projection. Applying the factor $-{}^1/_3$ yields a set of hyperfine values for the Fe(III) that is of the opposite sign to the intrinsic tensor. For a low-spin Fe(III), the intrinsic

DOI: 10.1021/acs.inorgchem.9b00746
Inorg. Chem. 2019, 58, 7069−7077

isotropic part of the tensor is negative, meaning that in this coupling scheme the observed A values yield a positive isotropic part. This is not the case in the **A** tensor obtained from the spectral fits with this coupling model; thus, the low-spin Fe(III) hypothesis is not consistent with the Mössbauer data. On the other hand, the projection coefficient for a spin coupling scheme in which $S_{Fe} = {}^3/_2$ and $S_{NO} = 1$ is given by $A_{ieff}(Fe{-}NO) = ({}^5/_3)A_{Fe} + (-{}^2/_3)A_{(NO)}$. In this case, it is expected that the effective A value of the intermediate-spin Fe^{3+}, A_{eff}, is larger than the intrinsic A value by a factor ${}^5/_3$ and it is of the same sign (negative). It should be noted that the same reasoning applied for the **A** tensor is valid for the **g** tensor. The available EPR data at room temperature are not conclusive in this regard. As indicated in Table 2, the g values of complex **1** are similar to those of the heme-NO complex Fe(TPP)(NO),[29] for which, to the best of our knowledge, no variable-field Mössbauer data or calculations have been published to support an unambiguous electron configuration of the Fe ion.

The Mössbauer spectra can also be fitted with a spin-coupled model in which an intermediate-spin Fe^{III} ion ($S_{Fe} = {}^3/_2$) is antiferromagnetically coupled ($J > 0$) with NO^- ($S_{NO} = 1$), yielding the required $S_{FeNO} = {}^1/_2$ ground state. (Figure SI-1) The Mössbauer spectral fits with the two-spin Hamiltonian demand that $D > 0$ for the Fe site but are insensitive to its magnitude, as long as $D \ll J$. This can be explained by considering the uncoupled representation, in which the effect of the **D** tensor appears as a second-order perturbation and can mix the $M_S = \pm{}^1/_2$ and $M_S = \pm{}^3/_2$ states. The amount of mixing is proportional to D/J. For an intermediate-spin ferric ion, for which D values can be between 2 and 30 cm^{-1},[11,45] coupled with the NO^- ($S = 1$) by a J value estimated by DFT to be on the order of 1000 cm^{-1},[38,46] it follows that $D \ll J$ and the mixing will be negligible regardless of D. Consequently, the ground state will be $S = {}^1/_2$; thus, the Mössbauer fits would not distinguish between the coupled model and the single $S = {}^1/_2$ model. Therefore, the $S = {}^1/_2$ model can be used without loss of information about the hyperfine interactions in complex **1**. Considering the $S = {}^1/_2$ overall spin of the $\{FeNO\}^7$ complex, the two lines of reasoning which argue against the low-spin Fe^{3+}, and the DFT calculations, we propose that the overall $S = {}^1/_2$ state of **1** is due to the strong antiferromagnetic coupling of an intermediate-spin Fe^{III} ($S_{Fe} = {}^3/_2$) to NO^- ($S = 1$). This assignment converges with the conclusions of Sun et al.,[7] which were based on sulfur K-edge spectra and theoretical calculations.

The main Mössbauer spectral features of the metallo-ligand were used in the analysis of the dinuclear $N_2S_2M(NO)$-Fe′(CO)Cp family (Figure 2). For complexes **2-A** and **3-A**, the Mössbauer spectra in high applied magnetic fields were well fitted with a diamagnetic ground state, which led to the conclusion that Ni^{II} and $\{CoNO\}^8$ do not interact in detectable ways with the low-spin $Fe'Cp(CO)^+$ center. However, when the metallo-ligand is the $\{Fe\text{-}NO\}^7$, i.e., for compound **1-A**, the spectra could not be fit without allowing the subspectrum of the Fe'_{Cp} to have splittings in addition to those from the nuclear Zeeman interaction. Thus, the simplest model that fits the spectra assumes that the effective spin $S_{tot} = {}^1/_2$ of the [Fe-NO] side (for which the hyperfine interactions are reported above) interacts with both the [FeNO] and the Fe'_{Cp} iron nuclei (Figure 4), yielding a small but noticeable magnetic hyperfine splitting at the Fe'_{Cp} nucleus. The corresponding Fermi contact contribution to the magnetic field at the iron nucleus can be estimated from the isotropic part of the **A** tensor, $A_{iso}/g_n\beta_n = (A_x + A_y + A_z)/3$, to be approximately 2.2 T (3 MHz), added to the applied magnetic field. Given that an unpaired 3d electron produces a Fermi contact contribution of approximately $A_F/g_n\beta_n = -12$ T (16.4 MHz), one would roughly estimate that for complex **1-A** the internal fields would correspond to 0.16 spin. This finding is in agreement with the results of the DFT calculations, which predict an isotropic part of the **A** tensor of 2.6 T (3.6 MHz), although the latter underestimates the spin density (0.02 spin) at the Fe'_{Cp} nucleus. Several instances of weak hyperfine interactions observed at nuclei of $S = 0$ low-spin Fe^{II} ions are found in the literature. Notable cases are the Fe^{II} centers of the [NiFe], [FeFe]- hydrogenases, and model complexes for the Fe^IFe^{II} state of the 2Fe subcluster.[47−52] Moreover, in a structurally and spectroscopically distinct pentanuclear complex in which low-spin Fe^{II} ions are bridging between paramagnetic Cr^{III} ions, the Fe^{II} nuclei were observed to show internal fields that could be attributed to polarization from neighboring Cr^{III} ions.[53]

The isomer shift of complex **1** and of the metallo-ligand [Fe-NO] in **1-A** is 0.23 mm/s, which is in the range of low-spin and intermediate-spin Fe^{III} complexes[38,45] and clearly smaller than those of high-spin $\{Fe\text{-}NO\}^7$ complexes.[10,33] On the other hand, the Fe'_{Cp} has an isomer shift of 0.35 mm/s, in agreement with the idea that within the $Fe{-}Fe'_{Cp}$ dimer, Fe'_{Cp} accepts electron density from the metallo-ligand, which was previously proposed on the basis of cyclic voltammetry and DFT calculations.[17]

The isomer shifts and quadrupole splittings were also estimated, according to the scheme introduced by Neese,[54] by computing the electron densities and electric-field gradients at the Fe nuclei. The isomer shift depends linearly on the nucleus electron density, but its precise quantification needs a dedicated calibration curve and a calibration constant, the latter of which shows moderate robustness to the variation of functionals and basis sets. The calibration constant, $\alpha = -0.367$ mm s^{-1} au^3, given by Neese with B3LYP and a triple-ζ quality basis set, was adopted here for semiquantitative, relative comparisons (Table SI-2). The two irons in **1-A** have distinguishable behaviors indicated by their very different coordination environments. Compared to that in the isolated metallo-ligand **1**, the Fe center in **1-A** has a more positive shift because of $Fe'(CO)Cp^+$ acting as an electron withdrawer, though the difference is within the typical experimental errors. On the other hand, the Mössbauer parameters of Fe'_{Cp} are not sensitive to the metal substitutions inside the N_2S_2 ligand, as confirmed by the calculations, though the replacement of $\{Fe(NO)\}^7$ in **1-A** with $\{Co(NO)\}^8$ or Ni^{II} causes the loss of paramagnetism in **2-A** and **3-A**.

This study offers new insights into the electronic structures of bimetallic complexes containing thiolate bridges between a low-spin Fe center and Fe-NO, Ni, and Co-NO centers. In particular, the Mössbauer analysis of [Fe-NO] complex **1** is presented and subsequently used to analyze the complicated spectroscopy of **1-A**. The Mössbauer spectra of compound **1-A** indicate that the low-spin Fe'_{Cp} ion exhibits weak hyperfine interactions, from interaction of the iron nucleus with the $S = {}^1/_2$ spin of the neighboring [Fe-NO]. It is notable that the series of bimetallics studied here were previously shown to exhibit electrocatalytic hydrogen evolution, with compound **1-A** being more stable during the electrocatalytic cycles, although

DOI: 10.1021/acs.inorgchem.9b00746
Inorg. Chem. 2019, 58, 7069−7077

no correlations are gleaned at this time between the hyperfine interactions determined in this study and the electrocatalytic activity.

■ ASSOCIATED CONTENT

Supporting Information

The Supporting Information is available free of charge on the ACS Publications website at DOI: 10.1021/acs.inorgchem.9b00746.

Tables with comparisons of the experimental and calculated metric parameters, experimental and computed zero-field Mössbauer parameters, computed magnetic hyperfine parameters, and additional Mössbauer parameters of complex **1** (PDF)

■ AUTHOR INFORMATION

Corresponding Authors

*E-mail: ewba2202@stthomas.edu.
*E-mail: hall@science.tamu.edu.

ORCID

Codrina V. Popescu: 0000-0003-2369-3383

Funding

The authors are grateful for financial support from National Science Foundation Grants NSF-RUI 1445959 (C.V.P.) and CHE-1300787 (M.B.H.) and Robert A. Welch Foundation Grant A-0648 (M.B.H.). Part of the experimental work (salary for Allen Lunsford and Pokhraj Ghosh) was made possible by an NPRP award (NPRP 6-1184-1-224) from the Qatar National Research Fund (a member of the Qatar Foundation). The authors acknowledge the Laboratory for Molecular Simulation at Texas A&M University for providing computing resources.

Notes

The authors declare no competing financial interest.

■ ACKNOWLEDGMENTS

The authors thank Dr. Marcetta Y. Darensbourg for making the compounds available for Mössbauer studies. The authors thank Dr. Sebastian Stoian (National Magnet Laboratory, University of Florida, presently at University of Idaho), Dr. Alex Guo (Carnegie Mellon University) for recording high-field Mössbauer spectra, and Dr. Michael P. Hendrich (Carnegie Mellon University) for the software Spin Count. The authors thank the reviewers for thoughtful and helpful comments which improved the manuscript.

■ REFERENCES

(1) Marsh, N.; Marsh, A. A Short History of Nitroglycerine and Nitric Oxide in Pharmacology and Physiology. *Clin. Exp. Pharmacol. Physiol.* **2000**, *27*, 313−319.

(2) Bredt, D. S.; Snyder, S. H. Nitric Oxide: A Physiologic Messenger Molecule. *Annu. Rev. Biochem.* **1994**, *63*, 175−195.

(3) Ding, H.; Demple, B. Direct Nitric Oxide Signal Transduction Via Nitrosylation of Iron-Sulfur Centers in the SoxR Transcription Activator. *Proc. Natl. Acad. Sci. U. S. A.* **2000**, *97* (10), 5146−5150.

(4) Moncada, S.; Palmer, R. M.; Higgs, E. A. Nitric Oxide: Physiology, Pathophysiology, and Pharmacology. *Pharmacol. Rev.* **1991**, *43*, 109−142.

(5) Snyder, S. H. Nitric Oxide: First in a New Class of Neurotransmitters. *Science* **1992**, *257*, 494−496.

(6) Collman, J. P.; Yang, Y.; Dey, A.; Decréau, R. A.; Ghosh, S.; Ohta, T.; Solomon, E. I. A Functional Nitric Oxide Reductase Model. *Proc. Natl. Acad. Sci. U. S. A.* **2008**, *105* (41), 15660−15665.

(7) Sun, N.; Liu, L. V.; Dey, A.; Villar-Acevedo, G.; Kovacs, J. A.; Darensbourg, M. Y.; Hodgson, K. O.; Hedman, B.; Solomon, E. I. S K-edge X-ray Absorption Spectroscopy and DFT Studies of High and Low Spin $\{FeNO\}^7$ Thiolate Complexes: Exchange Stabilization of Electron Delocalization in $\{FeNO\}^7$ and $\{FeO_2\}^8$. *Inorg. Chem.* **2011**, *50*, 427−436.

(8) Lehnert, N.; Scheidt, W. R.; Wolf, M. W. In *Nitrosyl Complexes in Inorganic Chemistry, Biochemistry and Medicine II*; Mingos, D. M. P., Ed.; Springer: Berlin, 2014; pp 155−223.

(9) Enemark, J. H.; Feltham, R. D. Principles of Structure, Bonding, and Reactivity for Metal Nitrosyl Complexes. *Coord. Chem. Rev.* **1974**, *13*, 339−406.

(10) Berto, T. C.; Speelman, A. L.; Zheng, S.; Lehnert, N. Mono-and Dinuclear Non-heme Iron-nitrosyl Complexes: Models for Key Intermediates in Bacterial Nitric Oxide Reductases. *Coord. Chem. Rev.* **2013**, *257*, 244−259.

(11) Hauser, C.; Glaser, T.; Bill, E.; Weyhermuller, T.; Wieghardt, K. The Electronic Structures of an Isostructural Series of Octahedral Nitrosyl-iron Complexes $\{Fe\text{-}NO\}^{6,7,8}$ Elucidated by Mössbauer Spectroscopy. *J. Am. Chem. Soc.* **2000**, *122*, 4352−4365.

(12) Praneeth, V. K. K.; Neese, F.; Lehnert, N. Spin Density Distribution in Five-and Six-Coordinated Iron(II)-Porphyrin NO Complexes Evidenced by Magnetic Circular Dichroism Spectroscopy. *Inorg. Chem.* **2005**, *44*, 2570−2572.

(13) Abbreviations: Bme-dach, *N*,*N*′-bis(2-mercaptoethyl)-1,4-diazacycloheptane; DNIC, dinitrosyl iron complexes; ligand L, 1,4,7-trimethyl-1,4,7-triazacyclononane; EDTA, ethylenediaminotetraacetic acid; TMG_3tren, 1,1,1-tris{2-[N^2-(1,1,3,3-tetramethyl)guanidino]ethyl}amine; EFG, electric-field gradient.

(14) Chiang, C.-Y.; Lee, J.; Dalrymple, C.; Sarahan, M. C.; Reibenspies, J. H.; Darensbourg, M. Y. Synthesis and Molecular Structures of Mononitrosyl $(N_2S_2)M(NO)$ Complexes (M = Fe, Co). *Inorg. Chem.* **2005**, *44* (24), 9007−9016.

(15) Ghosh, P.; Quiroz, M.; Wang, N.; Bhuvanesh, N.; Darensbourg, M. Y. Complexes of MN2S2·Fe(η^5-C_5R_5)(CO) as platform for exploring cooperative heterobimetallic effects in HER electrocatalysis. *Dalton Trans.* **2017**, *46*, 5617.

(16) Hsieh, C.-H.; Ding, S.; Erdem, O. F.; Crouthers, D. J.; Liu, T.; McCrory, C. C. L.; Lubitz, W.; Popescu, C. V.; Reibenspies, J. H.; Hall, M. B.; Darensbourg, M. Y. Redox Active Iron Nitrosyl Units in Proton Reduction Electrocatalysis. *Nat. Commun.* **2014**, *5*, 3684.

(17) Ding, S.; Ghosh, P.; Lunsford, A. M.; Wang, N.; Bhuvanesh, N.; Hall, M. B.; Darensbourg, M. Y. Hemilabile Bridging Thiolates as Proton Shuttles in Bioinspired H_2 Production Electrocatalysts. *J. Am. Chem. Soc.* **2016**, *138* (39), 12920−12927.

(18) Lubitz, W.; Reijerse, E.; van Gastel, M. [NiFe] and [FeFe] Hydrogenases Studied by Advanced Magnetic Resonance Techniques. *Chem. Rev.* **2007**, *107*, 4331−4365.

(19) Hess, J. L.; Conder, H. L.; Green, K. N.; Darensbourg, M. Y. Electronic Effects of $(N_2S_2)M(NO)$ Complexes (M = Fe, Co) as Metallodithiolate Ligands. *Inorg. Chem.* **2008**, *47* (6), 2056−2063.

(20) Del Castillo, T. J.; Thompson, N. B.; Peters, J. C. A Synthetic Single-site Fe Nitrogenase: High Turnover, Freeze-quench 57Fe Mössbauer Data, and a Hydride Resting State. *J. Am. Chem. Soc.* **2016**, *138* (16), 5341−5350.

(21) Neese, F. Software Update: The ORCA Program System. *WIREs Computational Molecular Science* **2012**, *8*, e1327.

(22) Ertl, G. Reactions at Surfaces: From Atoms to Complexity. *Angew. Chem., Int. Ed.* **2008**, *47*, 3524−3535.

(23) Ertl, G. Primary Steps in Catalytic Synthesis of Ammonia. *J. Vac. Sci. Technol., A* **1983**, *1*, 1247−1253.

(24) Smil, V. *Enriching the Earth*; MIT Press: Cambridge, MA, 2001.

(25) Boys, S. F. Construction of Some Molecular Orbitals to be Approximately Invariant for Changes from One Molecule to Another. *Rev. Mod. Phys.* **1960**, *32* (2), 296−299.

(26) Burgess, B. K.; Lowe, D. J. Mechanism of Molybdenum Nitrogenase. *Chem. Rev.* **1996**, *96*, 2983−3012.

(27) Einsle, O.; Tezcan, F. A.; Andrade, S. L. A.; Schmid, B.; Yoshida, M.; Howard, J. B.; Rees, D. C. Nitrogenase MoFe-protein at

DOI: 10.1021/acs.inorgchem.9b00746
Inorg. Chem. 2019, 58, 7069−7077

1.16 Å Resolution: A Central Ligand in the FeMo-cofactor. *Science* **2002**, *297*, 1696−1700.
(28) Howard, J. B.; Rees, D. C. Structural Basis of Biological Nitrogen Fixation. *Chem. Rev.* **1996**, *96*, 2965−2982.
(29) Nasri, H.; Ellison, M. K.; Chen, S.; Huynh, B. H.; Scheidt, W. R. Sharing the π-Bonding. An Iron Porphyrin Derivative with Trans, π-accepting Axial Ligands. Synthesis, EPR and Mössbauer Spectra, and Molecular Structure of Two Forms of the Complex Nitronitrosyl-(α,α,α,α-tetrakis(o-pivalamidophenyl)- Porphinato)Ferrate(II). *J. Am. Chem. Soc.* **1997**, *119*, 6274−6283.
(30) Franz, K. J.; Lippard, S. J. NO Disproportionation Reactivity of Fe Tropocoronand Complexes. *J. Am. Chem. Soc.* **1999**, *121* (45), 10504−10512.
(31) Ray, M.; Golombek, A. P.; Hendrich, M. P.; Yap, G. P. A.; Liable-Sands, L. M.; Rheingold, A. L.; Borovik, A. S. Structure and Magnetic Properties of Trigonal Bipyramidal Iron Nitrosyl Complexes. *Inorg. Chem.* **1999**, *38*, 3110−3115.
(32) Speelman, A. L.; Lehnert, N. Characterization of a High-spin Non-heme {FeNO}^{8} Complex: Implications for the Reactivity of Iron Nitroxyl Species in Biology. *Angew. Chem., Int. Ed.* **2013**, *52*, 12283−12287.
(33) Speelman, A. L.; Zhang, B.; Krebs, C.; Lehnert, N. Structural and Spectroscopic Characterization of a High-spin {FeNO}^{6} Complex with an Iron(IV)-NO$^-$ Electronic Structure. *Angew. Chem., Int. Ed.* **2016**, *55*, 6685−6688.
(34) Gibb, T. C.; Greatrex, R.; Greenwood, N. N.; Thompson, D. T. The Mössbauer Spectra of Some Phosphorous- and Sulphur-bridged Derivatives of Di-Iron Enneacarbonyl. *J. Chem. Soc. A* **1967**, *0*, 1663−1666.
(35) Chiang, C. Y.; Miller, M. L.; Reibenspies, J. H.; Darensbourg, M. Y. *J. Am. Chem. Soc.* **2004**, *126*, 10867−10874.
(36) Becke, A. D. A New Mixing of Hartree−Fock and Local Density-Functional Theories. *J. Chem. Phys.* **1993**, *98* (2), 1372−1377.
(37) Tao, J.; Perdew, J. P.; Staroverov, V. N.; Scuseria, G. E. Climbing the Density Functional Ladder: Nonempirical Meta-generalized Gradient Approximation Designed for Molecules and Solids. *Phys. Rev. Lett.* **2003**, *91* (14), 146401.
(38) Serres, R. G.; Grapperhaus, C. A.; Bothe, E.; Bill, E.; Weyhermüller, T.; Neese, F.; Wieghardt, K. Structural, Spectroscopic, and Computational Study of an Octahedral, Non-heme {Fe−NO}$^{6-8}$ Series: [Fe(NO)(cyclam-ac)]$^{2+/+/0}$. *J. Am. Chem. Soc.* **2004**, *126* (16), 5138−5153.
(39) Oosterhuis, W. T.; Lang, G. Mössbauer Effect in $K_3[Fe(CN)_6]$. *Phys. Rev.* **1969**, *178*, 439−456.
(40) Popescu, C. V. Mössbauer and EPR Studies of the H-Cluster of the Iron-Hydrogenases from C. pasteurianum and of Synthetic Complexes Designed to Model the Iron Sites of the $[Fe\text{-}Fe]_{(H)}$-Subcluster and Mössbauer Studies of the Transcription Factor FNR of *Escherichia coli*. Ph.D. Thesis, Carnegie Mellon University, Pittsburgh, PA, 2000.
(41) Popescu, C. V.; Münck, E.; Fox, B. G.; Sanakis, Y.; Cummings, J.; Turner, I. M.; Nelson, M. J. Mössbauer and EPR Studies of the Photoactivation of Nitrile Hydratase. *Biochemistry* **2001**, *40*, 7984−7991.
(42) Srivastava, J. K.; Bhargara, S. C.; Iyengar, P. K.; Thosar, B. V. *Introduction to Mössbauer Spectroscopy*; Elsevier: New York, 1983; pp 38−65.
(43) Münck, E. Mössbauer Spectroscoy of Proteins: Electron Carriers. *Methods Enzymol.* **1978**, *54*, 346−379.
(44) Kostka, K. L.; Fox, B. G.; Hendrich, M. P.; Collins, T. J.; Rickard, C. E. F.; Wright, L. J.; Münck, E. High-Valent Transition Metal Chemistry. Mössbauer and EPR Studies of High-Spin (S = 2) and Intermediate-Spin (S = 3/2) Iron (III) Complexes with a Macrocyclic Tetraamido-N Ligand. *J. Am. Chem. Soc.* **1993**, *115*, 6746−6757.
(45) Gutlich, P.; Bill, E.; Trautwein, A. X. *Mössbauer Spectroscopy and Transition Metal Chemistry*; Springer Verlag: Berlin, 2011; pp 417−425.
(46) Ghosh, P.; Bill, E.; Weyhermueller, T.; Neese, F.; Wieghardt, K. Noninnocence of the Ligand Glyoxal-bis(2-mercaptoanil). The Electronic Structures of $[Fe(gma)]_2$, [Fe(gma)(py)], [Fe(gma)-(CN)]$^{1-/0}$, [Fe(gma)I], and [Fe(gma)(PR_3)n] (n = 1, 2). Experimental and Theoretical Evidence for "Excited State" Coordination. *J. Am. Chem. Soc.* **2003**, *125*, 1293−1308.
(47) Erdem, Ö. F.; Schwartz, L.; Stein, M.; Silakov, A.; Kaur-Ghumaan, S.; Huang, P.; Ott, S.; Reijerse, E. J.; Lubitz, W. A Model of the [FeFe] Hydrogenase Active Site with a Biologically Relevant Azadithiolate Bridge: A Spectroscopic and Theoretical Investigation. *Angew. Chem., Int. Ed.* **2011**, *50* (6), 1439−1443.
(48) Huyett, J. E.; Carepo, M.; Pamplona, A.; Franco, R.; Moura, I.; Moura, J. J. G.; Hoffman, B. M. ^{57}Fe Q-band Pulsed ENDOR of the Hetero-dinuclear Site of Nickel Hydrogenase: Comparison of the NiA, NiB and NiC States. *J. Am. Chem. Soc.* **1997**, *119*, 9291.
(49) Pandelia, M. E.; Ogata, H.; Lubitz, W. Intermediates in the Catalytic Cycle of [NiFe] Hydrogenase: Functional Spectroscopy of the Active Site. *ChemPhysChem* **2010**, *11*, 1127−1140.
(50) Pereira, A. S.; Tavares, P.; Moura, J. J. G. M.; Moura, J. J. G.; Huynh, B. H. Mössbauer Characterization of the Iron-sulfur Clusters in Desulfovibrio Vulgaris Hydrogenase. *J. Am. Chem. Soc.* **2001**, *123*, 2771−2782.
(51) Popescu, C. V.; Münck, E. The Electronic Structure of the H Cluster in [Fe]-hydrogenases. *J. Am. Chem. Soc.* **1999**, *121*, 7877−7884.
(52) Stoian, S. A.; Hsieh, C.-H.; Casuras, A.; Singleton, M. L.; McNeely, K. M.; Darensbourg, M. Y.; Sweely, K.; Popescu, C. V. Hyperfine Interactions and Electron Distribution in $Fe^{II}Fe^{I}$ and $Fe^{I}Fe^{I}$ Models for the Active Site of the [FeFe]-hydrogenases: Mössbauer Spectroscopic Studies of Low-spin Fe^{I}. *JBIC, J. Biol. Inorg. Chem.* **2013**, *18* (6), 609−622.
(53) Shatruk, M.; Dragulescu-Andrasi, A.; Chambers, K. E.; Stoian, S. A.; Bominaar, E. L.; Achim, C.; Dunbar, K. R. Properties of Prussian Blue Materials Manifested in Molecular Complexes: Observation of Cyanide Linkage Isomerism and Spin-Crossover Behavior in Pentanuclear Cyanide Clusters. *J. Am. Chem. Soc.* **2007**, *129*, 6104−6116.
(54) Neese, F. Prediction and Interpretation of the ^{57}Fe Isomer Shift in Mössbauer Spectra by Density Functional Theory Calculations. *Inorg. Chim. Acta* **2002**, *337*, 181−192.

DOI: 10.1021/acs.inorgchem.9b00746
Inorg. Chem. 2019, 58, 7069−7077